

TruthLens: Visual Grounding for Universal DeepFake Reasoning

Rohit Kundu^{1,2}, Shan Jia², Vishal Mohanty², Athula Balachandran², Amit K. Roy-Chowdhury¹

¹University of California, Riverside; ²Google LLC

{rohit.kundu@email, amitrc@ece}.ucr.edu; {rohikun, shanjia, vishalmohanty, athula}@google.com



Figure 1: Illustration of Examples: Comparison of pretrained PaliGemma2 (Steiner et al. 2024) multimodal large language model's (MLLM) DeepFake reasoning against our proposed **TruthLens** framework on a face-manipulated image (left) and a fully AI-generated image (right). The pretrained PaliGemma2 fails to detect subtle inconsistencies in the manipulated images, resulting in incorrect explanations. In contrast, **TruthLens** provides accurate predictions along with detailed, fine-grained reasoning for the detected manipulations.

Abstract

Detecting DeepFakes has become a crucial research area as the widespread use of AI image generators enables the effortless creation of face-manipulated and fully synthetic content, while existing methods are often limited to binary classification (real vs. fake) and lack interpretability. To address these challenges, we propose **TruthLens**, a novel, unified, and highly generalizable framework that goes beyond traditional binary classification, providing detailed, textual reasoning for its predictions. Distinct from conventional methods, **TruthLens** performs MLLM grounding.

TruthLens uses a task-driven representation integration strategy that unites global semantic context from a multimodal large language model (MLLM) with region-specific forensic cues through explicit cross-modal adaptation of a vision-only model. This enables nuanced, region-grounded reasoning for both face-manipulated and fully synthetic content, and supports fine-grained queries such as “Does the eyes/nose/mouth look real or fake?” - capabilities beyond pretrained MLLMs alone. Extensive experiments across diverse datasets demonstrate that **TruthLens** sets a new benchmark in both forensic interpretability and detection accuracy, generalizing to seen and unseen manipulations alike. By unifying high-level scene understanding with fine-grained region grounding, **TruthLens** delivers transparent DeepFake forensics, bridging a critical gap in the literature.

Introduction

With accessible synthetic media generation tools (Labs 2024; Research 2023), hyper-realistic manipulated content can now be effortlessly created and are often difficult for hu-

mans to distinguish from authentic ones. Early DeepFakes primarily targeted face manipulations (Li et al. 2019; Thies, Zollhöfer, and Nießner 2019), but modern image-to-video (I2V) and text-to-video (T2V) models (Wang et al. 2023a; Research 2023; Zheng et al. 2024) enable synthesis of entire scenes and subjects. Current DeepFake detection frameworks (Cheng et al. 2024; Kundu et al. 2025) are mostly limited to binary (real/fake) classification of face-manipulated content. Achieving high classification accuracy, while valuable, does not address the urgent need for interpretable reasoning. For fostering trust in AI, DeepFake systems must go beyond black-box predictions and provide clear, grounded explanations for their decisions to aid forensic investigators.

Recently, multimodal large language models (MLLMs) have shown great promise for DeepFake reasoning (Jia et al. 2024; Shi et al. 2024). However, pretrained MLLMs are typically optimized for general-purpose tasks, such as image captioning (Anil et al. 2023; Liu et al. 2024) and visual question answering (Chen et al. 2024c,d), and lack the domain-specific adaptation required to reliably perform DeepFake reasoning (Chen et al. 2024b). Moreover, these models do not inherently ground their textual outputs in concrete visual evidence, which limits their interpretability in forensic settings, as seen in our evaluation of the pretrained PaliGemma2 (Steiner et al. 2024) MLLM (Figure 1).

To address these challenges, we introduce **TruthLens**, a universal DeepFake reasoning framework that goes beyond binary classification by performing MLLM grounding which couples fine-grained, interpretable textual reasoning with corresponding image regions. Unlike prior meth-

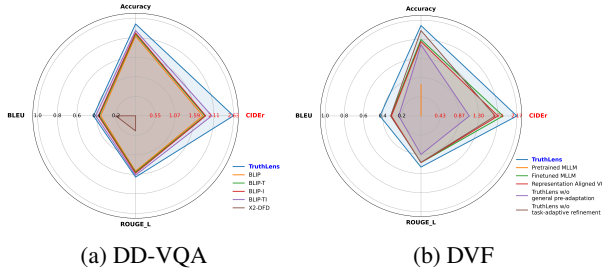


Figure 2: Comparison of [TruthLens](#) and state-of-the-art DeepFake reasoning methods on two benchmarks. (a) DD-VQA (Zhang et al. 2024) (face-manipulated) and (b) DVF (Song et al. 2024) (fully AI-generated): Black axis markings indicate scores for Accuracy, BLEU, and ROUGE_L, while red markings show the actual CIDEr score scale. [TruthLens](#) consistently outperforms competitors across all explanation and detection metrics, despite their specialization for face manipulation in (a) and significantly outperforms pretrained and simple finetuned MLLMs in (b), showing that our strategic grounding is essential for reasoning.

ods (Sun et al. 2025; Chen et al. 2024b) that are limited to face-manipulated data, *TruthLens* delivers region-level, visually grounded explanations for both face-manipulated and modern fully synthetic content (evident in Figures 1&2), answering nuanced forensic queries such as “Does the eyes/nose/mouth look real or fake?”

Existing DeepFake reasoning methods (Chen et al. 2024b; Guo et al. 2025) primarily fine-tune Vision-Language Models (VLMs), which tend to overlook subtle, localized manipulations due to their focus on global image context (Dahou et al. 2025; Tong et al. 2024). Off-the-shelf and simple finetuned MLLMs perform suboptimally in the DeepFake reasoning task in both face-manipulated and fully synthetic content as evident from Figure 2. Additionally, these methods require face-cropping as a preprocessing step, implicitly assuming consistently available front-view faces. In contrast, [TruthLens](#) leverages MLLM grounding with local context extraction using a vision-only model (VOM) to generalize across broader scenarios, including full-frame and non-frontal content, delivering detailed, region-specific reasoning without such restrictive preconditions.

The contributions of this work are as follows.

- We introduce [TruthLens](#), the first approach to achieve DeepFake-specific MLLM grounding aligning predictions with region-specific, visually anchored explanations, beyond global analyses with pretrained MLLMs.
- [TruthLens](#) surpasses binary classification by delivering fine-grained, query-driven, region-level explanations that provide forensic transparency.
- By uniting MLLM global context with localized features from a VOM, [TruthLens](#) achieves precise grounding for subtle manipulations often missed by existing VLMs.
- [TruthLens](#) generalizes robustly across both face manipulations and fully AI-generated content, surpassing SOTA in reasoning and detection across diverse datasets.

Related Work

Conventional DeepFake Detection: Early DeepFake detection methods (Li 2018; Yang, Li, and Lyu 2019) struggled with generalizability in cross-dataset settings, which is critical for in-the-wild detection. Dong et al. (Dong et al. 2023) tackled this issue by proposing an ID-unaware model that focuses on local image regions and employs an Artifact Detection Module to reduce identity bias, improving generalization. Methods like (Corvi et al. 2023b,a; Wang et al. 2023b; Chen et al. 2024a) address the synthetic content detection problem. Corvi et al. analyzed spectral (Corvi et al. 2023a) and frequency-domain (Corvi et al. 2023b) artifacts, such as spectral peaks and autocorrelation patterns, in diffusion-generated images, while Wang et al. (Wang et al. 2023b) proposed DIRE, leveraging reconstruction differences from pre-trained diffusion models to distinguish real from synthetic images with strong cross-model generalization. These methods focus on diffusion-generated images, and are not designed to handle the unique challenges of detecting facial DeepFakes. UNITE (Kundu et al. 2025) is the only method that performs DeepFake detection on all types of fake media (face/background manipulated and fully synthetic content) using a transformer architecture with “attention-diversity” loss. However, all of the aforementioned methods are designed only for binary classification tasks and cannot provide explanations like [TruthLens](#).

Visual Explainability: Most methods (Tăntăru, Oneață, and Oneață 2024; Xu, Raja, and Pedersen 2022) use Grad-CAM analysis to explain DeepFake detector predictions. However, Grad-CAM is insufficient, because it often highlights irrelevant or coarse regions, lacks fine-grained localization, making it less effective for pinpointing manipulated areas in DeepFake images. (Aghasani, Kangin, and Angelov 2023) used identity-specific features (prototypes) for DeepFake detection, and calculated Euclidean distance of the test images from the prototypes to infer which person’s DeepFake has been created. It fails in fine-grained localization and relies on identities used in training, making it ineffective for in-the-wild DeepFakes. In contrast, [TruthLens](#) provides precise, identity-agnostic explanations by pinpointing manipulated regions, delivering fine-grained reasoning without relying on predefined prototypes.

Text Explainability: Text-based DeepFake explainability provides fine-grained explanations more effectively than visual interpretability methods, as it can leverage natural language to articulate specific inconsistencies or manipulations in the content, offering detailed reasoning that is easier for humans to understand. However, there are very limited methods that integrate natural language with DeepFake Detection. (Jia et al. 2024; Shi et al. 2024) were early attempts that used ChatGPT (GPT-4V (Achiam et al. 2023)) and Gemini-1.0 (Anil et al. 2023) in zero-shot settings to detect face-manipulated images. DD-VQA (Zhang et al. 2024) finetuned the BLIP VLM (Li et al. 2022) to generate text explanations. Similarly, the \mathcal{X}^2 -DFD framework (Chen et al. 2024b) finetunes the LLaVA model (Liu et al. 2024). VLFFD (Sun et al. 2025) uses automatically generated visual-language prompts to guide detection and M2F2-Det (Guo et al. 2025) combines CLIP with an Vicuna-7b

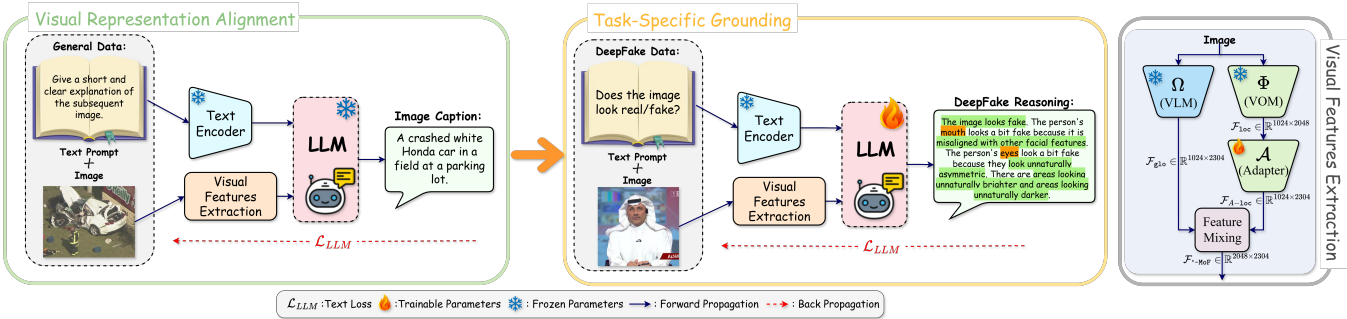


Figure 3: **Architecture of TruthLens**: To enable unified multimodal reasoning, local-context features from a vision-only model (Φ) are aligned to the language embedding space via a dedicated adapter (\mathcal{A}), while global-context features from a visual encoder (Ω) are directly fused as they are natively compatible with the LLM. The adapter is trained with a general image-caption dataset, ensuring that Φ ’s localized features capture fine-grained forensic details critical for DeepFake analysis. Subsequently, task-specific grounding is achieved by jointly optimizing \mathcal{A} and the LLM using language-annotated DeepFake data. This yields robust region-level grounding for both face manipulated and AI-generated content within a transparent, interpretable pipeline.

for face-manipulated content explanation. However, all of these methods detected and cropped the faces before analysis, assuming front-view human faces are always visible. Thus, they are not fit for fully-synthetic content explanation.

To the best of our knowledge, MM-Det (Song et al. 2024) and HEIE (Yang et al. 2025) are the only methods that attempted explainability in fully AI-generated content. MM-Det (Song et al. 2024) finetunes the LLaVA model (Liu et al. 2024) using their proposed text-annotated DVF dataset and HEIE (Yang et al. 2025) predominantly generate heatmaps and occasionally textual descriptions. These models cannot capture subtle inconsistencies and thus cannot detect face-manipulated DeepFakes. In contrast, **TruthLens** provides fine-grained, scenario-specific natural language explanations that articulate both where and how manipulations or inconsistencies occur. This enables users—especially human investigators—to understand the reasoning at a forensic, actionable level, not just spot potential artifacts.

Summary of Relation to Existing Work: Existing literature lacks a unified model capable of providing interpretable explanations for both face-manipulated DeepFakes and fully synthetic content. Moreover, even state-of-the-art pretrained MLLMs frequently overlook subtle, localized cues that are critical for reliable DeepFake detection, as illustrated in Figure 4. To address these limitations, we introduce **TruthLens**, a single framework for DeepFake reasoning that grounds its textual explanations in fine-grained visual evidence, enabling interpretable analysis of any manipulated content, whether face-centric or fully AI-generated.

Proposed Method

Problem Setup

Unlike existing methods (Chen et al. 2024b; Zhang et al. 2024; Sun et al. 2025; Guo et al. 2025) that focus solely on face-manipulated DeepFakes, our model provides a unified framework for explainability in both face-manipulated and fully AI-generated images. Given an image $\mathcal{I} \in \mathbb{R}^{H \times W \times 3}$ and a question \mathcal{Q} related to DeepFake detection, the objective of our model is to generate a detailed answer (ground

truth answer: \mathcal{E}) that determines whether the image is real or manipulated and provides an explanation for the decision. Our goal is to find the optimal parameters θ of our model f_θ that minimize the following objective function:

$$\arg \min_{\theta} \sum_{(\mathcal{I}, \mathcal{Q}, \mathcal{E}) \in \mathcal{D}} \mathcal{L}(f_\theta(\mathcal{I}, \mathcal{Q}), \mathcal{E}) \quad (1)$$

where \mathcal{D} is our training dataset of image-question-explanation triplets, and \mathcal{L} is a loss function measuring discrepancy between generated and ground truth explanations. This formulation enables our model to learn accurate, detailed explanations for DeepFake images.

Forensic Visual Grounding

Global Context: Effective DeepFake explanation requires comprehensive understanding of the visual and semantic coherence of an entire image, especially for fully synthetic content where manipulations often manifest as scene-level artifacts or implausible object arrangements. Capturing global context is crucial for detecting such abnormalities and generating meaningful, high-level explanations regarding overall authenticity. To address this, we utilize PaliGemma2 (Steiner et al. 2024), a state-of-the-art multimodal model that integrates advanced capabilities in both image and language understanding. The visual encoder (Ω) processes input images at a resolution of 448×448 and outputs a set of high-dimensional global visual tokens:

$$\mathcal{F}_{\text{glo}} = \Omega(\mathcal{I}^{448 \times 448 \times 3}) \quad (2)$$

where $\mathcal{F}_{\text{glo}} \in \mathbb{R}^{1024 \times 2304}$, yielding 1024 global tokens of 2304 dimensions each. These tokens capture holistic scene features and are projected into the LLM’s input space, forming a unified multimodal representation.

This strong aggregation of global context equips our system to recognize overarching inconsistencies, subtle compositional errors, and anomalous patterns in fully synthetic images, providing the foundational evidence necessary for robust and interpretable DeepFake forensics.



Figure 4: Pretrained MLLMs fail to ground forensic explanations to subtle manipulated regions. TruthLens, aided by localized context integration, surfaces minute attribute inconsistencies essential for reliable DeepFake interpretation.

Localized Context: A universal DeepFake explanation system must go beyond mere detection - it should pinpoint where manipulations occur and identify what attributes are affected, including subtle forensic cues often overlooked by conventional pretrained models. Standard VLMs, optimized for broad and global scene interpretation, systematically miss subtle cues: such as asymmetric eyes, unnaturally curved nose line, faint blending artifacts, etc. As visually shown in Figure 4, these overlooked regions can contain critical evidence essential for reliable forensic assessment — yet they are often missed when explanations rely solely on global context.

[TruthLens](#) directly addresses this deficit by capturing localized context at the level of image patches, rather than relying solely on global representations. Specifically, given an input image $I \in \mathbb{R}^{448 \times 448 \times 3}$, we partition it into $d \times d$ non-overlapping patches of size $p \times p$, with $p = 14$. Each patch is individually mapped into feature space, yielding embeddings as,

$$\mathcal{F}_{\text{loc}} = \Phi(\mathcal{I}^{448 \times 448 \times 3}) \in \mathbb{R}^{1024 \times 2048} \quad (3)$$

This dense, patch-wise encoding allows [TruthLens](#) to surface and ground explanations directly to regions such as [eyebrow](#), [nose](#), etc., which are prone to DeepFake traces yet often overlooked by pretrained MLLMs (as shown in Figure 4). Localized features empower the system to generate language that precisely pinpoints manipulations. Thus, our approach unifies region-specific forensic interpretability and holistic scene-level reasoning in a manner unattainable by conventional, purely global pipelines.

Cross-Modal Feature Adaptation and Fusion

A core challenge in universal DeepFake explanation is synthesizing visual evidence across disparate scales and modalities: pixel-level forensic irregularities and scene-level semantic coherence. Standard MLLMs excel at global compositional reasoning but systematically miss fine-grained manipulations, while vision-only models can expose subtle ar-

tifacts but lack alignment with natural language generation. Bridging this gap requires more than simple concatenation. It demands a principled approach to cross-modal feature alignment and integration.

Our approach models this fusion as a structured cross-modal adaptation pipeline. Since \mathcal{F}_{glo} and \mathcal{F}_{loc} reside in inherently incompatible feature spaces, we employ a learnable adapter \mathcal{A} , optimized specifically for high-fidelity modality alignment to project F_D into the LLM-compatible space:

$$\mathcal{F}_{A-\text{loc}} = \mathcal{A}(\mathcal{F}_{\text{loc}}) \in \mathbb{R}^{1024 \times 2304} \quad (4)$$

To form a unified and expressive representation, we combine these streams using an *interleaving* (I-MoF) strategy, where \mathcal{A} and Ω tokens alternate along the token dimension (and *concatenation* (C-MoF), as an ablation), where the sequences are joined as,

$$\mathcal{F}_{\text{I-MoF}}[k] = \begin{cases} \mathcal{F}_{\text{glo}}[j], & k = 2j - 1 \\ \mathcal{F}_{A-\text{loc}}[j], & k = 2j \end{cases} \quad (5)$$

$$j \in \{1, 2, \dots, 1024\}, k \in \{1, 2, \dots, 2048\}$$

$$\mathcal{F}_{\text{C-MoF}} = \mathcal{F}_{\text{glo}} \parallel \mathcal{F}_{A-\text{loc}} \quad (6)$$

where, for maximal architectural efficiency and minimal overfitting, we opt for unparameterized interleaving (or concatenation) rather than introducing additional fusion layers.

This design leverages the complementary strengths of each modality: Ω offers global semantic context for high-level reasoning, while adapted Φ features inject fine-grained forensic evidence critical for region-specific explanation. By tightly integrating these representations, our model is uniquely equipped to support both holistic scene-level understanding and the precise grounding of subtle, otherwise-missed manipulations, empowering region-grounded and interpretable explanations for universal DeepFake forensics within a single unified pipeline.

Explainability-Oriented Training

Effective forensic explainability demands more than generic pre-training and fine-tuning: the training process itself must be tailored to surface minute visual anomalies and map them to grounded, linguistically-coherent rationales. Our training regime therefore proceeds in two explicitly disentangled stages, each addressing a distinct explainability bottleneck.

Foundational Representation Alignment: We first calibrate \mathcal{A} within a large-scale multimodal grounding task, ensuring generalizable alignment of local visual features to the semantic space required by downstream language modeling. This phase leverages only foundational cross-modal signals, freezing the language model to avoid premature locking into task-specific distributions. To this end, we initialize \mathcal{A} on the large-scale LLaVA-Pretrain LCS-558K image-caption dataset (Liu et al. 2024). Here, the Gemma2 LLM remains frozen; only \mathcal{A} learns, via \mathcal{L}_{LLM} (objective explained in the next subsection) over generated captions, to map fine-grained Φ features into a modality space interpretable by the language tower using the fused representation \mathcal{F}_{MoF} . This diverse, caption-based pretraining equips the adapter with universal multimodal alignment, crucial for effective

downstream transfer and for preventing overfitting to specific DeepFake patterns.

The LCS-558K dataset (Liu et al. 2024) is widely used in literature (Huang et al. 2024; Peng et al. 2024; Nie et al. 2024) for training adapters in multimodal systems because it provides a large-scale, diverse collection of image-caption pairs. This diversity ensures that the adapter learns to generalize across a wide range of visual concepts and contexts, which is critical for downstream tasks requiring robust visual grounding and textual alignment. Furthermore, training on an image-captioning dataset aligns with the pretraining objectives of vision-language models, enabling effective integration of visual and textual modalities.

Task-Targeted Forensic Grounding: Building on this robust alignment, we progressively optimize both the adapter and LLM on richly annotated forensic datasets, jointly sculpting the visual-linguistic embedding space to surface subtle manipulations and map region-level evidence directly to natural language explanations. Here, optimization is guided by direct supervision from region and attribute-level forensics, enforcing precise semantic mapping between detected cues and their linguistic rationales.

This task-specific phase aligns the combined visual embeddings with nuanced forensic evidence, enabling the system to localize and lexically express subtle manipulations with high precision. Notably, keeping the adapter trainable during this stage is essential: ablation studies (Table 5) confirm that freezing \mathcal{A} impairs the model’s capacity to adapt to new, task-specific forensic cues.

Tokenization and Loss Computation: Each input question \mathcal{Q} and reference answer \mathcal{E} are tokenized (with τ) as,

$$\text{Prefix Tokens: } \mathcal{T}_{\text{prefix}} = \tau(\mathcal{Q}) \quad (7)$$

$$\text{Separator Token: } \mathcal{T}_{\text{separator}} = \tau(" \backslash n") \quad (8)$$

$$\text{Suffix Tokens: } \mathcal{T}_{\text{suffix}} = \tau(\mathcal{E}) \quad (9)$$

$$\text{Combined Tokens: } \mathcal{T} = \mathcal{T}_{\text{prefix}} \parallel \mathcal{T}_{\text{separator}} \parallel \mathcal{T}_{\text{suffix}} \quad (10)$$

We employ specialized attention, input, and loss masks to ensure cross-entropy optimization focuses exclusively on valid answer tokens, respecting both full and causal-attention requirements:

- **Attention Mask (\mathcal{M}_{ar}):** Specifies attention type for each token- full attention (0) for prefix (questions), causal attention (1) for suffix (answers), enabling autoregressive generation:

$$\mathcal{M}_{\text{ar}} = [0]^{|\mathcal{T}_{\text{prefix}}| + |\mathcal{T}_{\text{separator}}|} \parallel [1]^{|\mathcal{T}_{\text{suffix}}|} \quad (11)$$

- **Input Mask ($\mathcal{M}_{\text{input}}$):** Indicates valid tokens (1) and padding (0), ensuring only real data are processed as,

$$\mathcal{M}_{\text{input}} = [1]^{|\mathcal{T}|} \quad (12)$$

- **Loss Mask ($\mathcal{M}_{\text{loss}}$):** Ensures only answer (suffix) tokens contribute to the cross-entropy objective as,

$$\mathcal{M}_{\text{loss}} = [0]^{|\mathcal{T}_{\text{prefix}}| + |\mathcal{T}_{\text{separator}}|} \parallel [1]^{|\mathcal{T}_{\text{suffix}}|} \quad (13)$$

Thus, the loss objective becomes,

$$L_{\text{LLM}} = -\frac{\sum_{i=1}^{|\mathcal{T}|} \mathcal{M}_{\text{loss}}[i] \cdot \log P(\mathcal{T}[i])}{\sum_{i=1}^{|\mathcal{M}_{\text{loss}}|} \mathcal{M}_{\text{loss}}[i]} \quad (14)$$

Table 1: **SOTA Comparison on Face-Manipulated Data.** The methods used for the comparisons are specifically designed for face-manipulation detection. However our **TruthLens** framework is designed for both face-manipulated and synthetic content detection. DD-VQA (Zhang et al. 2024) is in-domain evaluation, all the other datasets are cross-data evaluations. **Best** and **second-best** performances are marked.

Dataset	Method	Accuracy	AUC	BLEU-4	ROUGE_L	CIDEr
DD-VQA (Zhang et al. 2024)	XceptionNet-BLIP-TI (Zhang et al. 2024)	89.25%	92.24%	-	-	-
	HiFiNet (Guo et al. 2023)	89.16%	92.10%	-	-	-
	HiFiNet-BLIP-TI (Zhang et al. 2024)	91.25%	95.14%	-	-	-
	RECCCE (Cao et al. 2022)	91.03%	95.02%	-	-	-
	RECCCE-BLIP (Zhang et al. 2024)	89.22%	93.71%	-	-	-
	RECCCE-BLIP-TI (Zhang et al. 2024)	92.08%	95.36%	-	-	-
	TruthLens	94.12%	95.39%	0.4304	0.6285	2.6321
	BLIP (Li et al. 2022)	83.65%	-	0.3569	0.5664	1.8177
	BLIP-1 (Zhang et al. 2024)	84.87%	-	0.3800	0.5882	1.8931
	BLIP-1 (Zhang et al. 2024)	87.49%	-	0.4075	0.6085	2.0567
	$\mathcal{X}^2\text{-DFD}$ (Chen et al. 2024b)	-	-	0.2030	0.1550	0.0270
CelebDF (Li et al. 2020)	TruthLens	92.86%	95.11%	0.3986	0.5481	2.1045
	XceptionNet-BLIP-TI (Zhang et al. 2024)	62.41%	64.30%	-	-	-
	HiFiNet (Guo et al. 2023)	67.20%	68.80%	-	-	-
	HiFiNet-BLIP-TI (Zhang et al. 2024)	69.37%	71.00%	-	-	-
	RECCCE (Cao et al. 2022)	67.96%	68.71%	-	-	-
	RECCCE-BLIP (Zhang et al. 2024)	68.07%	68.36%	-	-	-
	RECCCE-BLIP-TI (Zhang et al. 2024)	69.46%	70.21%	-	-	-
	TALL (Xu et al. 2023)	90.79%	-	-	-	-
	ISTV7 (Zhang et al. 2023)	84.10%	-	-	-	-
	Choi et al. (Choi et al. 2024)	89.00%	-	-	-	-
DF40 (Yan et al. 2024b)	$\mathcal{X}^2\text{-DFD}$ (Chen et al. 2024b)	-	91.30%	-	-	-
	VLFFD (Sun et al. 2025)	-	84.80%	-	-	-
	M2P2-Det (Guo et al. 2025)	-	95.10%	-	-	-
	TruthLens	99.58%	98.96%	0.4690	0.5395	2.3947

where $P(\cdot)$ is the predicted probability distribution over tokens. During inference, only $\mathcal{T}_{\text{prefix}}$ (question) is given, and the model generates output tokens autoregressively.

This explainability-oriented training protocol yields a modular, robust system, capable of both high-level scene reasoning and explicit, region-grounded forensic explanation, advancing the practical trustworthiness and interpretive power of **TruthLens** for DeepFake detection.

Experiments

Evaluation Metrics: We employ an LLM-as-a-judge mechanism using Gemini-1.0 (Anil et al. 2023) to evaluate **TruthLens**’s detection accuracy. Gemini compares the ground truth explanation with **TruthLens**’s prediction, providing a binary “yes” or “no” output to determine if they reach the same conclusion. This forms our LLM-as-a-judge detection accuracy metric. Additionally, we assess answer generation quality using standard natural language metrics following (Chen et al. 2024b; Zhang et al. 2024): BLEU_3, BLEU_4, ROUGE_L, and CIDEr. These metrics evaluate the fluency, coherence, and alignment of generated explanations with ground truth responses. This combined approach ensures a comprehensive assessment of both detection accuracy and explanation quality for **TruthLens**.

Training Details: **TruthLens** is trained using Stochastic Gradient Descent with an initial learning rate of 0.0001, scheduled to decay following a cosine annealing schedule. The training process is conducted with a batch size of 64 over 5 epochs for both representation alignment of Φ and task-targeted forensic grounding. Ω is the PaliGemma2 (Beyer et al. 2024) MLLM’s visual encoder, SigLIP-

Table 2: **SOTA Comparison on Synthetic Data:** SOTA models are trained and evaluated in-domain; **TruthLens** is trained on DD-VQA and DVF, with DVF in-domain and DeMamba for cross-dataset evaluation. **TruthLens** outperforms all baselines, including those trained on DeMamba. Competitors do not report answer generation metrics. **Best** and **second-best** results are marked.

Dataset	Method	Accuracy	AUC	BLEU.4	ROUGE.L	CIDEr
DVF (Song et al. 2024)	CNNDet (Wang et al. 2020)	-	78.20%	-	-	-
	DIRÉ (Wang et al. 2023b)	-	62.10%	-	-	-
	(Cozzolino et al. 2024)	-	67.00%	-	-	-
	UNI-FD (Qihui Li, and Lee 2023)	-	74.10%	-	-	-
	F3Net (Qian et al. 2020)	-	81.30%	-	-	-
	ViViT (Arnab et al. 2021)	-	79.10%	-	-	-
	TALL (Xu et al. 2023)	-	69.50%	-	-	-
	TS2-Net (Liu et al. 2022)	-	72.10%	-	-	-
	DE-FAKE (Shu et al. 2023)	-	72.10%	-	-	-
	HifiNet (Guo et al. 2023)	-	84.30%	-	-	-
	DVF (Song et al. 2024)	-	92.00%	-	-	-
TruthLens		94.47%	95.82%	0.4279	0.5338	2.1744
DeMamba (Chen et al. 2024a)	TALL (Xu et al. 2023)	88.42%	-	-	-	-
	F3Net (Qian et al. 2020)	86.04%	-	-	-	-
	NPR (Tao et al. 2024)	83.45%	-	-	-	-
	STL (Gu et al. 2021)	85.35%	-	-	-	-
	MINTIME-CLIP-B (Chen et al. 2024a)	89.97%	-	-	-	-
	FTCLIP-CLIP-B (Chen et al. 2024a)	89.67%	-	-	-	-
	CLIP-B-PT (Chen et al. 2024a)	41.82%	-	-	-	-
	DeMamba-CLIP-PT (Chen et al. 2024a)	70.98%	-	-	-	-
	XCLIP-B-PT (Chen et al. 2024a)	45.83%	-	-	-	-
	DeMamba-XCLIP-PT (Chen et al. 2024a)	79.31%	-	-	-	-
TruthLens		90.49%	92.67%	0.4165	0.5121	2.0619

So400m/14 (Alabdulmohsin et al. 2024), Φ is the DINOv2 (Oquab et al. 2023) vision-only foundation model and τ is the Gemma2 (Rivi  re et al. 2024) tokenizer in our case. \mathcal{A} is composed of one MLP layer following popular choices in the literature (Gao et al. 2024; Jiang et al. 2022). The framework is implemented in JAX and executed on 8 TPUv3 chips, ensuring efficient large-scale training.

TruthLens is trained on DD-VQA (Zhang et al. 2024) (face-manipulated FaceForensics++ or FF++ (Rossler et al. 2019) data annotated with language, resolution ablation in supplementary) and DVF (Song et al. 2024) (fully synthetic) datasets and evaluated on the following datasets:

- Face-manipulated: DD-VQA (Zhang et al. 2024), CelebDF (Li et al. 2020) and DF40 (Yan et al. 2024b)
- Fully synthetic: DVF (Song et al. 2024) and DeMamba (Chen et al. 2024a)

Except for DD-VQA and DVF, the other datasets lack language annotations. However, since class labels are available for these datasets and they are only used for evaluation, we manually design the question-answer pairs. Specifically, the questions are “Does the image look real or fake?”, and the corresponding answers are “The image looks `<real/fake>`,” to ensure consistency in evaluation.

State-of-the-art Comparison: **TruthLens**’s performance is evaluated against state-of-the-art (SOTA) methods for DeepFake detection on face-manipulated data (Table 1) and fully AI-generated data (Table 2). Existing SOTA methods are specialized for either face-manipulated or synthetic content detection, lacking the versatility to address both unlike our unified **TruthLens** framework.

Despite the more challenging cross-dataset evaluation, **TruthLens** consistently outperforms SOTA methods in both in-domain and cross-dataset settings. Notably, on DeMamba (Chen et al. 2024a), where baselines are trained and tested on the same data, **TruthLens** achieves superior results without seeing DeMamba during training, demon-

Table 3: **Pretrained vs. Grounded MLLM:** Performance comparison between pretrained and finetuned PaliGemma2 (Steiner et al. 2024). Although grounding PaliGemma2 improves performance **TruthLens** still performs better with its local context harvesting (as shown in Table 4).

Dataset	Grounded	Accuracy \uparrow	Face Manipulated Data			
			BLEU.3 \uparrow	BLEU.4 \uparrow	ROUGE.L \uparrow	CIDEr \uparrow
DD-VQA (Zhang et al. 2024)	✗	11.50%	0.0000	0.0000	0.0218	0.2610
	✓	88.19% (+76.69%)	0.4012 (+0.4012)	0.3768 (+0.3768)	0.5633 (+0.5415)	2.1478 (+1.8868)
CelebDF (Li et al. 2020)	✗	12.73%	0.0000	0.0000	0.0379	0.2549
	✓	85.38% (+72.65%)	0.3015 (+0.3015)	0.3445 (+0.3445)	0.4852 (+0.4473)	1.5617 (+1.3068)
DF40 (Yan et al. 2024b)	✗	0.32%	0.0000	0.0000	0.0009	0.0064
	✓	73.58% (+73.26%)	0.3031 (+0.3031)	0.3386 (+0.3386)	0.4019 (+0.4010)	1.6198 (+1.6134)
Synthetic Data						
DVF (Song et al. 2024)	✗	33.07%	0.0000	0.0000	0.0034	0.0001
	✓	79.88% (+46.81%)	0.3142 (+0.3142)	0.3839 (+0.3839)	0.4877 (+0.4843)	1.8629 (+1.8628)
DeMamba (Chen et al. 2024a)	✗	26.13%	0.0000	0.0000	0.0000	0.0428
	✓	86.81% (+60.68%)	0.3027 (+0.3027)	0.3698 (+0.3698)	0.4892 (+0.4892)	1.6729 (+1.6301)

Table 4: **Ablation on **TruthLens** Vision Features:** grounded SigLIP features, adapted DINOv2 features, C-MoF, and I-MoF (Ours) strategies. **Best** and **second-best** performances are marked.

Dataset	Features Used	Accuracy \uparrow	BLEU.3 \uparrow	BLEU.4 \uparrow	ROUGE.L \uparrow	CIDEr \uparrow
DD-VQA (Zhang et al. 2024)	SigLIP only	19.00%	0.3112	0.3768	0.5633	2.1478
	Adapted DINOv2 only	90.40%	0.4107	0.4443	0.6433	2.0616
	C-MoF	93.56%	0.4497	0.4296	0.6015	2.4193
	I-MoF (Ours)	94.12%	0.4649	0.4304	0.6285	2.6321
DVF (Song et al. 2024)	SigLIP only	79.88%	0.3142	0.3839	0.4877	1.8629
	Adapted DINOv2 only	77.67%	0.3077	0.3786	0.4873	1.7465
	C-MoF	92.81%	0.3614	0.4261	0.5234	2.1605
	I-MoF (Ours)	94.47%	0.3786	0.4279	0.5338	2.1744

ing strong generalization. Furthermore, **TruthLens** offers detailed textual explanations, enhancing interpretability.

Qualitative Results: Figure 5 demonstrates that **TruthLens** generates region-grounded, forensically relevant explanations for both fully synthetic and face-manipulated images. For facial DeepFakes, **TruthLens** localizes and articulates subtle manipulations, such as unnatural blending, asymmetric features, or fine textural anomalies, that pretrained MLLMs typically miss. As referenced in Figure 4, off-the-shelf MLLMs often overlook key attributes like eyes, mouth, or nose, which occupy a very small pixel area of the image, yielding only broad or generic rationales. In contrast, **TruthLens**’s localized context grounding enables it to identify and explain these nuanced artifacts. On fully synthetic images, it combines holistic and local cues, capturing both global anomalies (e.g., inconsistent color or lighting) and fine details.

Moreover, **TruthLens** consistently provides explanations that are more specific and relevant to the DeepFake task, whereas pretrained MLLMs generate generic/domain-irrelevant responses. By targeting manipulation-specific cues, **TruthLens** advances interpretable and trustworthy DeepFake forensics beyond generic, finetuned models.

Pretrained vs. Grounded MLLMs: We compare the performance of the pretrained and task-grounded PaliGemma2 model (without features from Φ) in Table 3. While the pretrained model demonstrates strong general-purpose reasoning, it falls short in DeepFake explainability. As shown in Figure 4, the pretrained MLLM failed to identify critical attributes such as eyes and mouth in the top face-manipulated image, and missed nose and subtle

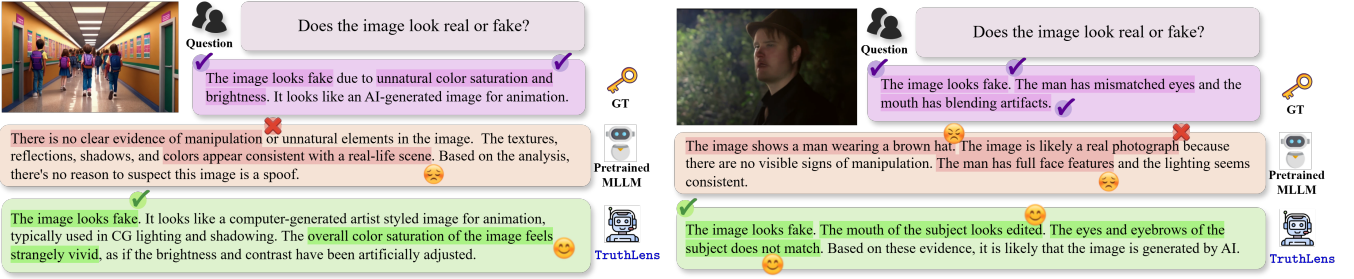


Figure 5: Examples demonstrating the DeepFake relevance of the responses generated by `TruthLens` compared to a pretrained MLLM (PaliGemma2). Our method not only enhances accuracy on DeepFake detection, but also improves relevance to the task including various DeepFake-specific finegrained reasonings.

Table 5: **Ablation on Adapter Configurations.**

Dataset	Adapter Settings	Accuracy ↑	BLEU.3 ↑	BLEU.4 ↑	ROUGE.L ↑	CIDEr ↑
Face-Manipulated Data						
DD-VQA (Zhang et al. 2024)	No general pre-adaptation	79.13%	0.3017	0.2975	0.5113	1.5812
	No task-adaptive refinement	86.56%	0.3964	0.3897	0.5712	2.0447
	Joint training only	90.371%	0.4106	0.3946	0.6375	2.3186
	TruthLens	94.12%	0.4649	0.4304	0.6285	2.6321
CelebDF (Li et al. 2020)	No general pre-adaptation	71.32%	0.2173	0.2617	0.3950	1.2934
	No task-adaptive refinement	81.4%	0.2934	0.3315	0.5065	1.7156
	Joint training only	88.13%	0.3185	0.3413	0.5246	1.8221
	TruthLens	92.86%	0.3578	0.3986	0.5485	2.1045
DF40 (Yan et al. 2024b)	No general pre-adaptation	80.0%	0.1521	0.1616	0.2481	0.6833
	No task-adaptive refinement	92.71%	0.2664	0.3318	0.4259	1.3193
	Joint training only	91.73%	0.3015	0.3716	0.4816	1.7163
	TruthLens	99.58%	0.3998	0.4690	0.5395	2.3947
Synthetic Data						
DVF (Song et al. 2024)	No general pre-adaptation	74.39%	0.2317	0.2815	0.4014	1.0961
	No task-adaptive refinement	89.23%	0.3173	0.3681	0.4844	1.6820
	Joint training only	114.41%	(0.0760)	(0.0656)	(0.0532)	(0.5539)
	TruthLens	119%	0.3350	0.3875	0.4972	1.8988
DeMamba (Chen et al. 2024a)	No general pre-adaptation	66.25%	0.2315	0.3109	0.4017	1.0416
	No task-adaptive refinement	81.79%	0.3016	0.3763	0.4368	1.5633
	Joint training only	115.54%	(0.0701)	(0.0654)	(0.0531)	(0.5217)
	TruthLens	96.54%	0.3281	0.3865	0.4833	1.8154

blending artifacts in the bottom example. Grounding the model on domain-specific DeepFake data substantially enhances its ability to surface forensic evidence, underscoring the need for explicit adaptation of MLLMs like PaliGemma2 to specialized detection scenarios. This grounding process enables the model to recognize and align with task-relevant cues and subtle manipulations, ultimately achieving higher accuracy and interpretability in line with forensic requirements.

Ablation study on Feature Mixing: We perform an ablation study to assess the importance of different features and their mixing strategies within `TruthLens`, as detailed in Table 4, using the DD-VQA and DVF datasets. Using Ω or \mathcal{A} features alone leads to inferior results compared to the MoF approach. Furthermore, the interleaved MoF strategy outperforms simple concatenation, highlighting that interleaving, by keeping global and local context aligned per 14×14 spatial patch (which is inherent to both Ω VLM and Φ VOM), yields superior feature integration and overall performance.

The performance differences between Ω and \mathcal{A} highlight the varying importance of global versus localized features. For face-manipulated data like DD-VQA, where manipulations are confined to small pixel regions, features from \mathcal{A} are

more effective than Ω -derived global features. Conversely, for fully synthetic data such as DVF, which requires understanding global context across the entire frame, Ω features outperform \mathcal{A} features. This underscores the need for a hybrid approach in `TruthLens` to balance both global and localized feature representations effectively.

Ablation on Adapter: Table 5 summarizes different adapter training strategies:

1. *No general pre-adaptation*: The adapter is aligned only on DD-VQA & DVF and remains fixed thereafter.
2. *No task-adaptive refinement*: The adapter is pretrained on LCS-558K but is not updated on downstream tasks.
3. *Joint training only*: The adapter and LLM are optimized together on DeepFake data without separate alignment.

These configurations are compared against our progressive adaptation framework, where the adapter is first aligned with general multimodal semantics on LCS-558K (Liu et al. 2024), then further specialized for DeepFake forensics via joint optimization with the LLM on domain-specific data. This targeted adaptation outperforms all alternatives by uniting broad visual-linguistic grounding with task-specific sensitivity. Setting-1 fails to leverage broad multimodal learning, Setting-2 lacks forensic specialization, and Setting-3 misses foundational feature calibration. By balancing universal representation and task adaptation, `TruthLens` achieves robust and generalizable performance across diverse DeepFake scenarios.

Conclusion

In this work, we present `TruthLens`, a task-driven framework for DeepFake detection that unifies global semantic context from a MLLM with localized forensic cues extracted from a VOM. Through explicit cross-modal adaptation and grounding, `TruthLens` delivers nuanced, region-level textual explanations alongside state-of-the-art detection accuracy. Extensive evaluations across varied datasets confirm its superior ability to capture subtle manipulations in both face-manipulated and fully AI-generated content, establishing new benchmarks in forensic interpretability and robustness. By bridging high-level scene understanding with fine-grained visual grounding, `TruthLens` advances the development of trustworthy, transparent DeepFake systems.

References

Achiam, J.; Adler, S.; Agarwal, S.; Ahmad, L.; Akkaya, I.; Aleman, F. L.; Almeida, D.; Altenschmidt, J.; Altman, S.; Anadkat, S.; et al. 2023. Gpt-4 technical report. *arXiv preprint arXiv:2303.08774*.

Aghasanli, A.; Kangin, D.; and Angelov, P. 2023. Interpretable-through-prototypes deepfake detection for diffusion models. In *Proceedings of the IEEE/CVF international conference on computer vision*, 467–474.

Alabdulmohsin, I. M.; Zhai, X.; Kolesnikov, A.; and Beyer, L. 2024. Getting vit in shape: Scaling laws for compute-optimal model design. *Advances in Neural Information Processing Systems*, 36.

Anil, R.; Borgeaud, S.; Alayrac, J.-B.; Yu, J.; Soricut, R.; Schalkwyk, J.; Dai, A. M.; Hauth, A.; Millican, K.; et al. 2023. Gemini: a family of highly capable multimodal models. *arXiv preprint arXiv:2312.11805*.

Arnab, A.; Dehghani, M.; Heigold, G.; Sun, C.; Lučić, M.; and Schmid, C. 2021. Vivit: A video vision transformer. In *Proceedings of the IEEE/CVF international conference on computer vision*, 6836–6846.

Beyer, L.; Steiner, A.; Pinto, A. S.; Kolesnikov, A.; Wang, X.; Salz, D.; Neumann, M.; Alabdulmohsin, I.; Tschannen, M.; Bugliarello, E.; et al. 2024. PaliGemma: A versatile 3B VLM for transfer. *arXiv preprint arXiv:2407.07726*.

Cao, J.; Ma, C.; Yao, T.; Chen, S.; Ding, S.; and Yang, X. 2022. End-to-end reconstruction-classification learning for face forgery detection. In *Proceedings of the IEEE/CVF Conference on Computer Vision and Pattern Recognition*, 4113–4122.

Chen, H.; Hong, Y.; Huang, Z.; Xu, Z.; Gu, Z.; Li, Y.; Lan, J.; Zhu, H.; Zhang, J.; Wang, W.; et al. 2024a. DeMamba: AI-Generated Video Detection on Million-Scale GenVideo Benchmark. *arXiv preprint arXiv:2405.19707*.

Chen, Y.; Yan, Z.; Lyu, S.; and Wu, B. 2024b. \mathcal{X}^2 -DFD: A framework for e \mathcal{X} plainable and e \mathcal{X} tendable Deepfake Detection. *arXiv preprint arXiv:2410.06126*.

Chen, Z.; Wang, W.; Tian, H.; Ye, S.; Gao, Z.; Cui, E.; Tong, W.; Hu, K.; Luo, J.; Ma, Z.; et al. 2024c. How far are we to gpt-4v? closing the gap to commercial multimodal models with open-source suites. *Science China Information Sciences*, 67(12): 220101.

Chen, Z.; Wu, J.; Wang, W.; Su, W.; Chen, G.; Xing, S.; Zhong, M.; Zhang, Q.; Zhu, X.; Lu, L.; et al. 2024d. Internvl: Scaling up vision foundation models and aligning for generic visual-linguistic tasks. In *Proceedings of the IEEE/CVF Conference on Computer Vision and Pattern Recognition*, 24185–24198.

Cheng, J.; Yan, Z.; Zhang, Y.; Luo, Y.; Wang, Z.; and Li, C. 2024. Can We Leave Deepfake Data Behind in Training Deepfake Detector? *arXiv preprint arXiv:2408.17052*.

Choi, J.; Kim, T.; Jeong, Y.; Baek, S.; and Choi, J. 2024. Exploiting Style Latent Flows for Generalizing Deepfake Video Detection. In *Proceedings of the IEEE/CVF Conference on Computer Vision and Pattern Recognition*, 1133–1143.

Corvi, R.; Cozzolino, D.; Poggi, G.; Nagano, K.; and Verdoliva, L. 2023a. Intriguing properties of synthetic images: from generative adversarial networks to diffusion models. In *Proceedings of the IEEE/CVF Conference on Computer Vision and Pattern Recognition*, 973–982.

Corvi, R.; Cozzolino, D.; Zingarini, G.; Poggi, G.; Nagano, K.; and Verdoliva, L. 2023b. On the detection of synthetic images generated by diffusion models. In *ICASSP 2023-2023 IEEE International Conference on Acoustics, Speech and Signal Processing (ICASSP)*, 1–5. IEEE.

Cozzolino, D.; Poggi, G.; Corvi, R.; Nießner, M.; and Verdoliva, L. 2024. Raising the Bar of AI-generated Image Detection with CLIP. In *Proceedings of the IEEE/CVF Conference on Computer Vision and Pattern Recognition*, 4356–4366.

Dahou, Y.; Huynh, N. D.; Le-Khac, P. H.; Para, W. R.; Singh, A.; and Narayan, S. 2025. Vision-Language Models Can't See the Obvious. *arXiv preprint arXiv:2507.04741*.

Dong, S.; Wang, J.; Ji, R.; Liang, J.; Fan, H.; and Ge, Z. 2023. Implicit identity leakage: The stumbling block to improving deepfake detection generalization. In *Proceedings of the IEEE/CVF Conference on Computer Vision and Pattern Recognition*, 3994–4004.

Gao, P.; Geng, S.; Zhang, R.; Ma, T.; Fang, R.; Zhang, Y.; Li, H.; and Qiao, Y. 2024. Clip-adapter: Better vision-language models with feature adapters. *International Journal of Computer Vision*, 132(2): 581–595.

Gu, Z.; Chen, Y.; Yao, T.; Ding, S.; Li, J.; Huang, F.; and Ma, L. 2021. Spatiotemporal inconsistency learning for deepfake video detection. In *Proceedings of the 29th ACM international conference on multimedia*, 3473–3481.

Guo, X.; Liu, X.; Ren, Z.; Grosz, S.; Masi, I.; and Liu, X. 2023. Hierarchical fine-grained image forgery detection and localization. In *Proceedings of the IEEE/CVF Conference on Computer Vision and Pattern Recognition*, 3155–3165.

Guo, X.; Song, X.; Zhang, Y.; Liu, X.; and Liu, X. 2025. Rethinking Vision-Language Model in Face Forensics: Multi-Modal Interpretable Forged Face Detector. In *Proceedings of the Computer Vision and Pattern Recognition Conference*, 105–116.

Huang, B.; Wang, X.; Chen, H.; Song, Z.; and Zhu, W. 2024. Vtimellm: Empower llm to grasp video moments. In *Proceedings of the IEEE/CVF Conference on Computer Vision and Pattern Recognition*, 14271–14280.

Huang, B.; Wang, Z.; Yang, J.; Ai, J.; Zou, Q.; Wang, Q.; and Ye, D. 2023. Implicit identity driven deepfake face swapping detection. In *Proceedings of the IEEE/CVF conference on computer vision and pattern recognition*, 4490–4499.

Jia, S.; Lyu, R.; Zhao, K.; Chen, Y.; Yan, Z.; Ju, Y.; Hu, C.; Li, X.; Wu, B.; and Lyu, S. 2024. Can chatgpt detect deepfakes? a study of using multimodal large language models for media forensics. In *Proceedings of the IEEE/CVF Conference on Computer Vision and Pattern Recognition*, 4324–4333.

Jiang, H.; Zhang, J.; Huang, R.; Ge, C.; Ni, Z.; Lu, J.; Zhou, J.; Song, S.; and Huang, G. 2022. Cross-modal adapter for text-video retrieval. *arXiv preprint arXiv:2211.09623*.

Kundu, R.; Xiong, H.; Mohanty, V.; Balachandran, A.; and Roy-Chowdhury, A. K. 2025. Towards a Universal Synthetic Video Detector: From Face or Background Manipulations to Fully AI-Generated Content. *Proceedings of the IEEE/CVF Conference on Computer Vision and Pattern Recognition*.

Labs, B. 2024. FLUX 1.1. <https://blackforestlabs.ai/>.

Li, J.; Li, D.; Xiong, C.; and Hoi, S. 2022. Blip: Bootstrapping language-image pre-training for unified vision-language understanding and generation. In *International conference on machine learning*, 12888–12900. PMLR.

Li, L.; Bao, J.; Yang, H.; Chen, D.; and Wen, F. 2019. Faceshifter: Towards high fidelity and occlusion aware face swapping. *arXiv preprint arXiv:1912.13457*.

Li, Y. 2018. Exposing deepfake videos by detecting face warping artif acts. *arXiv preprint arXiv:1811.00656*.

Li, Y.; Yang, X.; Sun, P.; Qi, H.; and Lyu, S. 2020. Celeb-df: A large-scale challenging dataset for deepfake forensics. In *Proceedings of the IEEE/CVF conference on computer vision and pattern recognition*, 3207–3216.

Lin, Y.; Song, W.; Li, B.; Li, Y.; Ni, J.; Chen, H.; and Li, Q. 2024. Fake it till you make it: Curricular dynamic forgery augmentations towards general deepfake detection. In *European Conference on Computer Vision*, 104–122. Springer.

Liu, H.; Li, C.; Wu, Q.; and Lee, Y. J. 2024. Visual instruction tuning. *Advances in neural information processing systems*, 36.

Liu, Y.; Xiong, P.; Xu, L.; Cao, S.; and Jin, Q. 2022. Ts2-net: Token shift and selection transformer for text-video retrieval. In *European conference on computer vision*, 319–335. Springer.

Ni, Y.; Meng, D.; Yu, C.; Quan, C.; Ren, D.; and Zhao, Y. 2022. Core: Consistent representation learning for face forgery detection. In *Proceedings of the IEEE/CVF conference on computer vision and pattern recognition*, 12–21.

Nie, M.; Ding, D.; Wang, C.; Guo, Y.; Han, J.; Xu, H.; and Zhang, L. 2024. SlowFocus: Enhancing Fine-grained Temporal Understanding in Video LLM. In *The Thirty-eighth Annual Conference on Neural Information Processing Systems*.

Ojha, U.; Li, Y.; and Lee, Y. J. 2023. Towards universal fake image detectors that generalize across generative models. In *Proceedings of the IEEE/CVF Conference on Computer Vision and Pattern Recognition*, 24480–24489.

Oquab, M.; Darcet, T.; Moutakanni, T.; Vo, H.; Szafraniec, M.; Khalidov, V.; Fernandez, P.; Haziza, D.; Massa, F.; El-Nouby, A.; et al. 2023. Dinov2: Learning robust visual features without supervision. *arXiv preprint arXiv:2304.07193*.

Peng, T.; Li, Z.; Zhang, L.; Zhao, H.; Wang, P.; and Du, B. 2024. Multi-modal Auto-regressive Modeling via Visual Tokens. In *Proceedings of the 32nd ACM International Conference on Multimedia*, MM '24, 10735–10744. New York, NY, USA: Association for Computing Machinery. ISBN 9798400706868.

Qian, Y.; Yin, G.; Sheng, L.; Chen, Z.; and Shao, J. 2020. Thinking in frequency: Face forgery detection by mining frequency-aware clues. In *European conference on computer vision*, 86–103. Springer.

Research, R. 2023. Text driven video generation. <https://research.runwayml.com/gen2>.

Rivi  re, M.; Pathak, S.; Sessa, P. G.; Hardin, C.; Bhupatiraju, S.; Hussenot, L.; Mesnard, T.; Shahriari, B.; Ram  , A.; Ferret, J.; et al. 2024. Gemma 2: Improving Open Language Models at a Practical Size. *CoRR*.

Rossler, A.; Cozzolino, D.; Verdoliva, L.; Riess, C.; Thies, J.; and Nie  ner, M. 2019. Faceforensics++: Learning to detect manipulated facial images. In *Proceedings of the IEEE/CVF international conference on computer vision*, 1–11.

Sha, Z.; Li, Z.; Yu, N.; and Zhang, Y. 2023. De-fake: Detection and attribution of fake images generated by text-to-image generation models. In *Proceedings of the 2023 ACM SIGSAC Conference on Computer and Communications Security*, 3418–3432.

Shi, Y.; Gao, Y.; Lai, Y.; Wang, H.; Feng, J.; He, L.; Wan, J.; Chen, C.; Yu, Z.; and Cao, X. 2024. Shield: An evaluation benchmark for face spoofing and forgery detection with multimodal large language models. *arXiv preprint arXiv:2402.04178*.

Shiohara, K.; and Yamasaki, T. 2022. Detecting deepfakes with self-blended images. In *Proceedings of the IEEE/CVF conference on computer vision and pattern recognition*, 18720–18729.

Song, X.; Guo, X.; Zhang, J.; Li, Q.; Bai, L.; Liu, X.; Zhai, G.; and Liu, X. 2024. On learning multi-modal forgery representation for diffusion generated video detection. *The Thirty-eighth Annual Conference on Neural Information Processing Systems*.

Steiner, A.; Pinto, A. S.; Tschannen, M.; Keysers, D.; Wang, X.; Bitton, Y.; Gritsenko, A.; Minderer, M.; Sherbondy, A.; Long, S.; et al. 2024. Paligemma 2: A family of versatile vlms for transfer. *arXiv preprint arXiv:2412.03555*.

Sun, K.; Chen, S.; Yao, T.; Zhou, Z.; Ji, J.; Sun, X.; Lin, C.-W.; and Ji, R. 2025. Towards general visual-linguistic face forgery detection. In *Proceedings of the Computer Vision and Pattern Recognition Conference*, 19576–19586.

Tan, C.; Zhao, Y.; Wei, S.; Gu, G.; Liu, P.; and Wei, Y. 2024. Rethinking the up-sampling operations in cnn-based generative network for generalizable deepfake detection. In *Proceedings of the IEEE/CVF Conference on Computer Vision and Pattern Recognition*, 28130–28139.

Thies, J.; Zollh  fer, M.; and Nie  ner, M. 2019. Deferred neural rendering: Image synthesis using neural textures. *AcM Transactions on Graphics (TOG)*, 38(4): 1–12.

Tong, S.; Liu, Z.; Zhai, Y.; Ma, Y.; LeCun, Y.; and Xie, S. 2024. Eyes wide shut? exploring the visual shortcomings of multimodal llms. In *Proceedings of the IEEE/CVF Conference on Computer Vision and Pattern Recognition*, 9568–9578.

Wang, J.; Yuan, H.; Chen, D.; Zhang, Y.; Wang, X.; and Zhang, S. 2023a. Modelscope text-to-video technical report. *arXiv preprint arXiv:2308.06571*.

Wang, S.-Y.; Wang, O.; Zhang, R.; Owens, A.; and Efros, A. A. 2020. CNN-generated images are surprisingly easy to

spot... for now. In *Proceedings of the IEEE/CVF conference on computer vision and pattern recognition*, 8695–8704.

Wang, Z.; Bao, J.; Zhou, W.; Wang, W.; Hu, H.; Chen, H.; and Li, H. 2023b. Dire for diffusion-generated image detection. In *Proceedings of the IEEE/CVF International Conference on Computer Vision*, 22445–22455.

Xu, Y.; Liang, J.; Jia, G.; Yang, Z.; Zhang, Y.; and He, R. 2023. Tall: Thumbnail layout for deepfake video detection. In *Proceedings of the IEEE/CVF international conference on computer vision*, 22658–22668.

Xu, Y.; Raja, K.; and Pedersen, M. 2022. Supervised contrastive learning for generalizable and explainable deepfakes detection. In *Proceedings of the IEEE/CVF Winter Conference on Applications of Computer Vision*, 379–389.

Yan, Z.; Luo, Y.; Lyu, S.; Liu, Q.; and Wu, B. 2024a. Transcending forgery specificity with latent space augmentation for generalizable deepfake detection. In *Proceedings of the IEEE/CVF Conference on Computer Vision and Pattern Recognition*, 8984–8994.

Yan, Z.; Yao, T.; Chen, S.; Zhao, Y.; Fu, X.; Zhu, J.; Luo, D.; Yuan, L.; Wang, C.; Ding, S.; et al. 2024b. DF40: Toward Next-Generation Deepfake Detection. *NeurIPS 2024*.

Yan, Z.; Zhang, Y.; Fan, Y.; and Wu, B. 2023. Ucf: Uncovering common features for generalizable deepfake detection. In *Proceedings of the IEEE/CVF International Conference on Computer Vision*, 22412–22423.

Yang, F.; Zhen, R.; Wang, J.; Zhang, Y.; Chen, H.; Lu, H.; Zhao, S.; and Ding, G. 2025. Heie: Milm-based hierarchical explainable aigc image implausibility evaluator. In *Proceedings of the Computer Vision and Pattern Recognition Conference*, 3856–3866.

Yang, X.; Li, Y.; and Lyu, S. 2019. Exposing deep fakes using inconsistent head poses. In *ICASSP 2019-2019 IEEE International Conference on Acoustics, Speech and Signal Processing (ICASSP)*, 8261–8265. IEEE.

Zhang, Y.; Colman, B.; Guo, X.; Shahriyari, A.; and Bharaj, G. 2024. Common sense reasoning for deepfake detection. In *European Conference on Computer Vision*, 399–415. Springer.

Zhao, C.; Wang, C.; Hu, G.; Chen, H.; Liu, C.; and Tang, J. 2023. ISTVT: interpretable spatial-temporal video transformer for deepfake detection. *IEEE Transactions on Information Forensics and Security*, 18: 1335–1348.

Zheng, Z.; Peng, X.; Yang, T.; Shen, C.; Li, S.; Liu, H.; Zhou, Y.; Li, T.; and You, Y. 2024. Open-Sora: Democratizing Efficient Video Production for All.

Tăntaru, D.-C.; Oneață, E.; and Oneață, D. 2024. Weakly-supervised deepfake localization in diffusion-generated images. In *Proceedings of the IEEE/CVF Winter Conference on Applications of Computer Vision*, 6258–6268.

Reproducibility Checklist

Instructions for Authors:

This document outlines key aspects for assessing reproducibility. Please provide your input by editing this `.tex` file directly.

For each question (that applies), replace the “Type your response here” text with your answer.

Example: If a question appears as

```
\question{Proofs of all novel claims  
are included} { (yes/partial/no) }  
Type your response here
```

you would change it to:

```
\question{Proofs of all novel claims  
are included} { (yes/partial/no) }  
yes
```

Please make sure to:

- Replace ONLY the “Type your response here” text and nothing else.
- Use one of the options listed for that question (e.g., **yes**, **no**, **partial**, or **NA**).
- **Not** modify any other part of the `\question` command or any other lines in this document.

You can `\input` this `.tex` file right before `\end{document}` of your main file or compile it as a stand-alone document. Check the instructions on your conference’s website to see if you will be asked to provide this checklist with your paper or separately.

1. General Paper Structure

1. Includes a conceptual outline and/or pseudocode description of AI methods introduced (yes/partial/no/NA) **yes**
2. Clearly delineates statements that are opinions, hypothesis, and speculation from objective facts and results (yes/no) **yes**
3. Provides well-marked pedagogical references for less-familiar readers to gain background necessary to replicate the paper (yes/no) **yes**

2. Theoretical Contributions

- 2.1. Does this paper make theoretical contributions? (yes/no) **no**
If yes, please address the following points:
 - 2.2. All assumptions and restrictions are stated clearly and formally (yes/partial/no) **NA**
 - 2.3. All novel claims are stated formally (e.g., in theorem statements) (yes/partial/no) **NA**
 - 2.4. Proofs of all novel claims are included (yes/partial/no) **NA**

- 2.5. Proof sketches or intuitions are given for complex and/or novel results (yes/partial/no) **NA**
- 2.6. Appropriate citations to theoretical tools used are given (yes/partial/no) **NA**
- 2.7. All theoretical claims are demonstrated empirically to hold (yes/partial/no/NA) **NA**
- 2.8. All experimental code used to eliminate or disprove claims is included (yes/no/NA) **NA**

3. Dataset Usage

- 3.1. Does this paper rely on one or more datasets? (yes/no) **yes**

If yes, please address the following points:

- 3.2. A motivation is given for why the experiments are conducted on the selected datasets (yes/partial/no/NA) **yes**
- 3.3. All novel datasets introduced in this paper are included in a data appendix (yes/partial/no/NA) **NA**
- 3.4. All novel datasets introduced in this paper will be made publicly available upon publication of the paper with a license that allows free usage for research purposes (yes/partial/no/NA) **NA**
- 3.5. All datasets drawn from the existing literature (potentially including authors' own previously published work) are accompanied by appropriate citations (yes/no/NA) **yes**
- 3.6. All datasets drawn from the existing literature (potentially including authors' own previously published work) are publicly available (yes/partial/no/NA) **yes**
- 3.7. All datasets that are not publicly available are described in detail, with explanation why publicly available alternatives are not scientifically satisfying (yes/partial/no/NA) **NA**

4. Computational Experiments

- 4.1. Does this paper include computational experiments? (yes/no) **yes**

If yes, please address the following points:

- 4.2. This paper states the number and range of values tried per (hyper-) parameter during development of the paper, along with the criterion used for selecting the final parameter setting (yes/partial/no/NA) **yes**
- 4.3. Any code required for pre-processing data is included in the appendix (yes/partial/no) **no**
- 4.4. All source code required for conducting and analyzing the experiments is included in a code appendix

(yes/partial/no) **no**

- 4.5. All source code required for conducting and analyzing the experiments will be made publicly available upon publication of the paper with a license that allows free usage for research purposes (yes/partial/no) **no**
- 4.6. All source code implementing new methods have comments detailing the implementation, with references to the paper where each step comes from (yes/partial/no) **no**
- 4.7. If an algorithm depends on randomness, then the method used for setting seeds is described in a way sufficient to allow replication of results (yes/partial/no/NA) **yes**
- 4.8. This paper specifies the computing infrastructure used for running experiments (hardware and software), including GPU/CPU models; amount of memory; operating system; names and versions of relevant software libraries and frameworks (yes/partial/no) **yes**
- 4.9. This paper formally describes evaluation metrics used and explains the motivation for choosing these metrics (yes/partial/no) **yes**
- 4.10. This paper states the number of algorithm runs used to compute each reported result (yes/no) **yes**
- 4.11. Analysis of experiments goes beyond single-dimensional summaries of performance (e.g., average; median) to include measures of variation, confidence, or other distributional information (yes/no) **no**
- 4.12. The significance of any improvement or decrease in performance is judged using appropriate statistical tests (e.g., Wilcoxon signed-rank) (yes/partial/no) **no**
- 4.13. This paper lists all final (hyper-)parameters used for each model/algorithm in the paper's experiments (yes/partial/no/NA) **yes**